

# Dose-dependent reduction of cardiac transmembrane potential by high-intensity electrical shocks

MICHEL NEUNLIST<sup>1</sup> AND LESLIE TUNG<sup>2</sup>

<sup>1</sup>Department of Physiology, School of Veterinary Medicine of Hannover, 30173 Hannover, Germany; and <sup>2</sup>Department of Biomedical Engineering, The Johns Hopkins University, Baltimore, Maryland 21205

**Neunlist, Michel, and Leslie Tung.** Dose-dependent reduction of cardiac transmembrane potential by high-intensity electrical shocks. *Am. J. Physiol.* 273 (*Heart Circ. Physiol.* 42): H2817–H2825, 1997.—Cardiac tissue dysfunction can result from high-intensity electrical shocks and is manifested as changes in transmembrane potential ( $V_m$ ). Ten-millisecond shock pulses (SPs) of varying intensity and polarity were applied to frog ventricle in diastole, and  $V_m$  was quantified directly under the stimulating electrode by an optical method using voltage-sensitive dye. As SP intensities were increased, the shock-induced action potential (AP) plateau and AP amplitude ( $APA_s$ ) decreased sigmoidally toward 75–85% of the control AP amplitude ( $APA_c$ ) and zero, respectively.  $APA_s$  was shifted toward lower current densities for anodal compared with cathodal SPs (half-maximal values 185 and 238 mA/cm<sup>2</sup>, respectively;  $P = 0.02$ ). Recovery of  $APA_s$  was marginally significant 1 s after SP delivery ( $P = 0.063$ ). The peak change in  $V_m$  during SP (across all intensity levels) was  $-200\%$   $APA_c$  for anodal and  $+125\%$   $APA_c$  for cathodal pulses. In conclusion, we show that SP reduces APA in a sigmoidal fashion at strengths  $>10$ – $20 \times$  diastolic threshold and is more deleterious for anodal polarities.

cardiac tissue; voltage-sensitive dye; anodal shock; cathodal shock; extracellular electrode; electroporation

THE USE OF ELECTRICAL PULSES as a means for treating various cardiac arrhythmias has increased in the past 15 years. The therapeutic applications of electrical pulses range from cardiac pacing to defibrillation and also encompass antiarrhythmic pacing, cardioversion, and ablation. The rate of success of this treatment depends on various parameters, such as the pulse intensity and duration, the waveform used, the position of the shock electrodes, and the physiological state of the heart. For example, the probability of successful defibrillation follows a bell-shaped curve as a function of increasing current intensity (9), first increasing and then decreasing with increasing current densities of the shock. The decreased efficacy at higher intensities has been attributed to postshock cellular dysfunction and refrillation (9). In addition, cardioversion or ablation can sometimes reinitiate ventricular tachycardia after the shock (7). Therefore, the deleterious effects of high-intensity electrical shocks may be tissue dysfunction produced by the large current pulses (27), which is most serious under or near the stimulating electrode, where the current densities are the largest and the electric field is highly nonuniform (22, 32, 33). The nature of the alterations induced by high-intensity pulses has been identified at different structural levels in the heart (27). At the tissue level, these effects may include changes in threshold from pacemakers, in-

crease in defibrillation threshold after multiple shocks, induction of ventricular tachycardia, S-T segment change, conduction block, and metabolic change. At the cellular level electrical shocks can alter the rise time, duration, and amplitude of the action potential.

Clearly, it is important to characterize the level of electrical toxicity. However, precise determination of a dysfunctional threshold is hampered by experimental observations that dysfunction, however it is defined, varies in a graded fashion with the shock parameters (e.g., intensity, duration, waveform shape, and number of shocks; 27). As a rough guideline, however, levels of local electrical field sufficient to induce dysfunction have been estimated in previous experimental studies to be in the range of 15–80 V/cm, depending on the type of dysfunction and experimental preparation. A major limitation with the use of local electric field as a parameter is that it is difficult to measure without a separate electrode array and cannot be measured adjacent to the stimulating electrode. On the other hand, current density at the electrode surface is a parameter that in practice can be determined (neglecting edge effects) from the total current passing through the electrode and the electrode surface area. Unfortunately, estimates of the dysfunction level in terms of local current density are sparse and in one study have been estimated to be in the range of 500 mA/cm<sup>2</sup> (for damped sinusoidal pulses to produce mild arrhythmia) to 1.8 A/cm<sup>2</sup> (to produce irreversible cell damage; 14). The goal of this study, therefore, was to quantitate the graded increase in dysfunction (indexed here as changes in action potential parameters) with increasing local current density.

One mechanism of tissue damage that has been postulated to be produced by high-intensity pulses is membrane electroporation (27). It has been shown that when the transmembrane potential ( $V_m$ ) induced by an electrical field reaches a critical value, a rapid and enormous increase occurs in membrane conductance. This increase in conductance is attributed to the formation of pores in the membrane (10, 18, 25) that allow the indiscriminate exchange of ions, enzymes, and even macromolecules between the extracellular and intracellular domains. This process tends to depolarize the cells and can induce cell death by calcium overload (28). If electroporation is in fact the mechanism that underlies electrical dysfunction, one would expect that during diastole (where  $V_m$  is "biased" at a resting level of about  $-85$  mV) the same level of dysfunction would occur at lower current densities for hyperpolarizing (anodal) compared with depolarizing (cathodal) shocks. Hence,

part of this study was directed at testing this hypothesis.

To our knowledge, no study to date has reported the change in  $V_m$  in tissue subjacent to the shock delivery electrode during and following the application of high-intensity pulses. The main reason is a technical one. With conventional recording techniques (microelectrode) it is very difficult to record changes in  $V_m$  free of electrical artifacts in the vicinity of the stimulating electrode, much less underneath the electrode where the stimulating currents are high. The use of voltage-sensitive fluorescent dyes presents an adequate solution to this problem. Voltage-sensitive dyes can measure changes in  $V_m$  (20) and allow electrical artifact-free recordings even during high-intensity electrical pulses (15). Our approach employs an optical fiber to collect the fluorescent light directly under an extracellular stimulating electrode (17), during and following the shock pulse.

Thus we present in this paper strength-duration curves for the detrimental effects of electrical pulses with varying intensity and polarity on the action potential in myocardial tissue. Preliminary results have been presented in abstract form (30).

## METHODS

**Preparation.** All experiments were performed at room temperature (20–25°C) on isolated ventricles of the frog heart (*Rana pipiens*). After the heart was isolated, the ventricle was incubated in Ringer solution containing 30  $\mu\text{M}$  4-(2-(6-(dibutylamino)-2-naphthalenyl)ethenyl)-1-(3-sulfo-propyl)-pyridinium hydroxide, inner salt (di-4-ANEPPS; Molecular Probes, Eugene, OR; from 10 mM stock solution in 100% dimethyl sulfoxide) for 10–15 min. After the staining procedure, the ventricle was washed out with normal Ringer solution. Details concerning the mounting procedure and solutions have been described previously (15).

**Stimulus electrode.** A glass suction pipette was filled with Ringer solution and connected to a stimulator (model SD9, Grass Instruments, Quincy, MA) by a Ag-AgCl wire. It served as the stimulating electrode and was inserted in a modified microelectrode holder mounted onto a micromanipulator as previously described (15). The tip radius of the pipette used in our experiments was 150  $\mu\text{m}$ . The amplitude of the stimulus current was monitored by the voltage drop across a resistor (100  $\Omega$  or 1 k $\Omega$ ) in series with the electrode. Because the inner diameter of the tip of the stimulating pipette was known, the average current density was determined as the ratio between applied current and total cross-sectional area of the tip. It is possible that the current density was not strictly uniform across the tip cross section because boundary effects at the electrode edge due to current spread to the adjacent volume conductor would result in higher current densities there. Therefore, the use of average current density could potentially underestimate the peak current density under the electrode. Nonetheless, such errors would have been systematic and would not be expected to invalidate the major conclusions of this study. The reference electrode was a 1-mm-diameter Ag-AgCl electrode placed in the bath away from the ventricle.

**Optical setup.** The optical setup has been previously described (17). In brief, it consists of a single, multimode optical fiber (diameter 140  $\mu\text{m}$ ) interfaced to a custom-built fluorimeter. The free end of the fiber is abutted against a heart

stained with the voltage-sensitive dye di-4-ANEPPS. The fiber carries excitation light to the heart surface and also collects the fluorescent signal, which is then converted to an electrical signal by a photodiode and current-to-voltage amplifier with a 3-kHz bandwidth. The fiber can be threaded inside the lumen of the stimulating pipette so that  $V_m$  can be recorded directly under the stimulating electrode. It is important to note that the optical signal is derived from a volume of tissue  $\sim 200$   $\mu\text{m}$  in diameter and is a signal integrated over many cells. Slight suction was also applied to the lumen of the stimulus electrode to immobilize the heart-fiber optic interface. We have shown previously that this procedure can be used to obtain recordings free of motion artifacts (17). The multimode glass optical fiber was adjusted to a distance of  $\sim 100$   $\mu\text{m}$  from the tissue for two reasons: it improved the magnitude of the signal (17), and it allowed current to flow unimpeded to the tissue.

**Experimental protocol.** First, the cathodal diastolic threshold of excitation (DT) was determined by an up-down-up procedure. The intensity of a 10-ms cathodal pulse was increased in steps of  $\sim 0.2$  V until an action potential was induced. The intensity of the pulse was then reduced in steps of  $\sim 0.1$  V until a subthreshold response was obtained, and finally the intensity was increased until threshold was reached again. This final value was considered to be the DT and was used to normalize the level of shock intensity. Once the DT was determined, a shock pulse (SP) was applied during diastole. The SP was a 10-ms, rectangular, constant-current pulse, either cathodal or anodal in polarity. To determine whether recovery occurred shortly after the shock, we sometimes delivered a test pulse (TP) 1 s after the SP to generate another action potential. The TP was always a 10-ms, rectangular, constant-current anodal pulse with amplitude  $\sim 6 \times$  DT. For shocks with intensity greater than  $\sim 50 \times$  DT, the tissue was allowed to recover for 5–10 min between shocks. Multiple trials were performed on the same heart, and shocks were applied at sites at least 2 mm apart to avoid cumulative and interactive effects.

**Curve fits.** Data for the measured parameters followed sigmoidal relationships. Fits were obtained using a least-squares method (Kaleidagraph, Synergy Software, Reading, PA) applied to

$$f(J) = 1 - \frac{aJ^b}{J^b + c^b} \quad (1)$$

where  $J$  is the current density (mA/cm<sup>2</sup>),  $1 - a$  is the amplitude of function  $f$  for  $J = \infty$ ,  $b$  is the slope coefficient, and  $c$  is the current density value at half-maximum.

**Statistical methods.** The dependence of the dose-response curves on stimulus polarity was analyzed by analysis of covariance (SAS 6.03; SAS Institute, Cary, NC) of a subset of all the data points, with polarity as the grouping factor and shock intensity as the covariate. The subset was chosen to be those points lying on the approximately linear portion of the sigmoidal relation, in the range between 20 and 80% of the interval from 1 to  $(1 - a)$  for Eq. 1. Shifts in the data after a 1-s recovery time were calculated as a recovery index (RI, defined in RESULTS) and tested first for dependence on shock strength by determining the correlation coefficient  $r$  for a linear fit, and second for significance as a group against the null hypothesis of no recovery using the Student's paired  $t$ -test. In addition, comparison between proportions was performed using the  $z$  test to test the difference of the recovery index as a function of the shock polarity. Values of  $P < 0.05$  were considered to be significant in all cases.

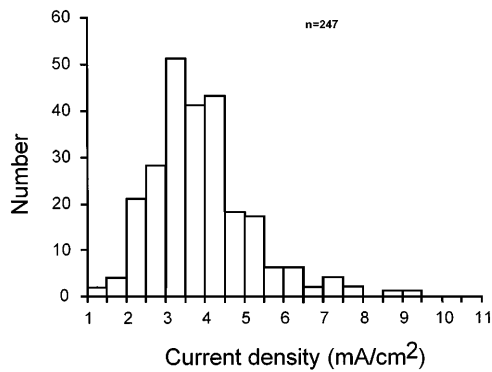


Fig. 1. Histogram of the pulse current density at the cathodal diastolic threshold of excitation (DT) for a 10-ms rectangular constant-current pulse. A total of 247 measurements were made in 20 frog ventricles with a 150- $\mu$ m-diameter stimulating electrode. Mean current density at DT was  $3.9 \pm 1.3$  mA/cm<sup>2</sup>.

## RESULTS

A total of 247 DTs were measured, and 210 SPs were delivered to 20 isolated frog ventricles. The histogram of DT current density is plotted in Fig. 1, and the mean ( $\pm$ SE) was found to be  $3.9 \pm 1.3$  mA/cm<sup>2</sup> ( $2.8 \pm 0.9$   $\mu$ A in absolute units). The effects of the SPs on action potential characteristics measured directly under the stimulating electrode are illustrated in Fig. 2, A-D. A control action potential elicited with a cathodal pulse of  $1.5 \times$  DT intensity is superimposed on each response induced by the shock. With higher levels of current, there was a progressive decrease in the amplitude of the action potential plateau (APP) and a rise in the resting potential (RP). The changes in the test action potential initiated by the TP are similar to those of the SP-induced action potential, with a decrease in its amplitude resulting from an increase in SP current density (Fig. 2, A-D).

**Parameters.** Figure 3 graphically shows the various parameters of the SP- and TP-induced action potentials that were measured as a function of stimulus current density. These parameters are defined as follows:  $APA_c$

is the amplitude of the control action potential measured 100 ms after the upstroke, initiated by a 10-ms cathodal pulse with intensity of  $\sim 1.5 \times$  DT;  $\Delta V_{mp}$  is the peak  $V_m$  induced during an SP of intensity  $J$  (in mA/cm<sup>2</sup>) relative to RP and is normalized to  $APA_c$ ;  $\Delta V_{me}$  is the  $V_m$  measured at the end of an SP of intensity  $J$  (in mA/cm<sup>2</sup>) relative to RP and is normalized to  $APA_c$ ; APP is the action potential plateau of  $V_m$  measured 100 ms after the shock and is normalized to  $APA_c$ ;  $RP_s$  is the relative amplitude of the RP measured  $\sim 1$  s after SP and is normalized to  $APA_c$ ;  $APA_s$  is the action potential amplitude initiated by an SP having an intensity  $J$  (in mA/cm<sup>2</sup>), measured as the difference between APP and  $RP_s$  and normalized to  $APA_c$ ; and  $APA_t$  is the action potential amplitude induced by a TP after an SP of intensity  $J$  (in mA/cm<sup>2</sup>).  $APA_t$  is measured 100 ms after the TP and is normalized to  $APA_c$ . The TP was an anodal pulse of intensity  $\sim 6 \times$  DT.

**APP as a function of current density and pulse polarity.** A total of 108 cathodal and 102 anodal SPs was applied, ranging in intensity  $J$  from 16 mA/cm<sup>2</sup> ( $\sim 4 \times$  DT) to 1,300 mA/cm<sup>2</sup> ( $\sim 425 \times$  DT). Figure 4 illustrates APP for anodal and cathodal pulses as a function of  $J$ . For both pulse polarities, the APPs decreased sigmoidally with increasing shock intensity from a value of 1 to about 0.8 and were fit by a function of the form of Eq. 1. The subsets of data falling within the 20–80% values of the vertical range of the curve fit were then used to define the linear portions of the sigmoidal relations. These subsets were subjected to analysis of covariance, and the difference between the 50% effective doses ( $ED_{50}$ ), i.e., half-maximal points of the data, was found to be statistically significant (94 mA/cm<sup>2</sup> and 145 mA/cm<sup>2</sup> for anodal and cathodal data, respectively;  $P = 0.0001$ ). Therefore, on average the cathodal pulses require a higher intensity to induce a comparable change in APP than did the anodal pulses.

**$RP_s$  as a function of current density and pulse polarity.** One difficulty encountered during the measurement of  $RP_s$  was the presence of motion artifacts that appeared sometimes at higher shock intensities, i.e.,

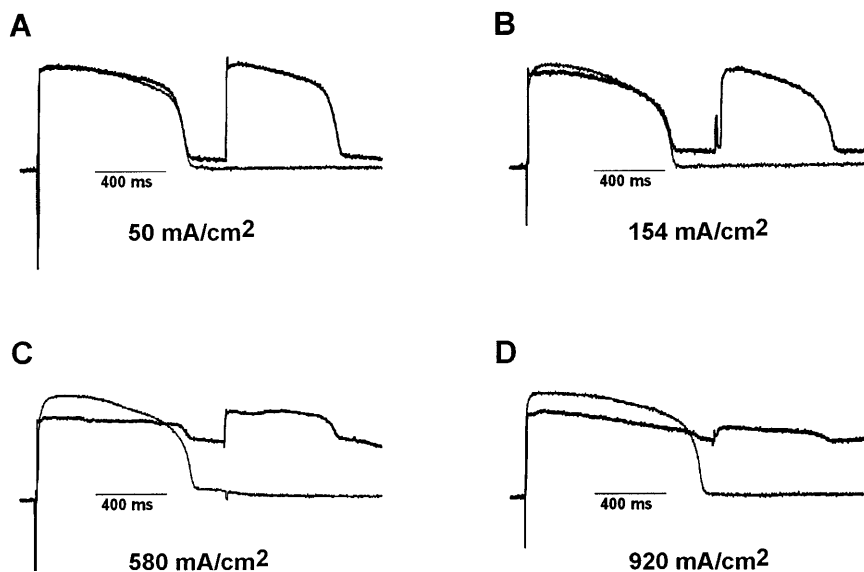


Fig. 2. Typical effect of increasing shock pulse (SP) intensity on action potential morphology. In A-D, a control action potential is superposed on the action potential induced by SP and followed, 1 s after SP, by a test action potential. A: anodal SP of 50 mA/cm<sup>2</sup> does not produce any noticeable change in action potential characteristics except for a reduction in the magnitude of the resting potential ( $RP_s$ ). B: anodal SP of 154 mA/cm<sup>2</sup> produces a further decrease in  $RP_s$ , a decrease in the amplitude of the action potential plateau (APP), and a decrease in test action potential amplitude ( $APA_t$ ). C: anodal SP of 580 mA/cm<sup>2</sup> produces a substantial decrease in  $RP_s$ , APP, and  $APA_t$ . D: anodal SP of 920 mA/cm<sup>2</sup> produces a further decrease in  $RP_s$ , APP, and  $APA_t$ .

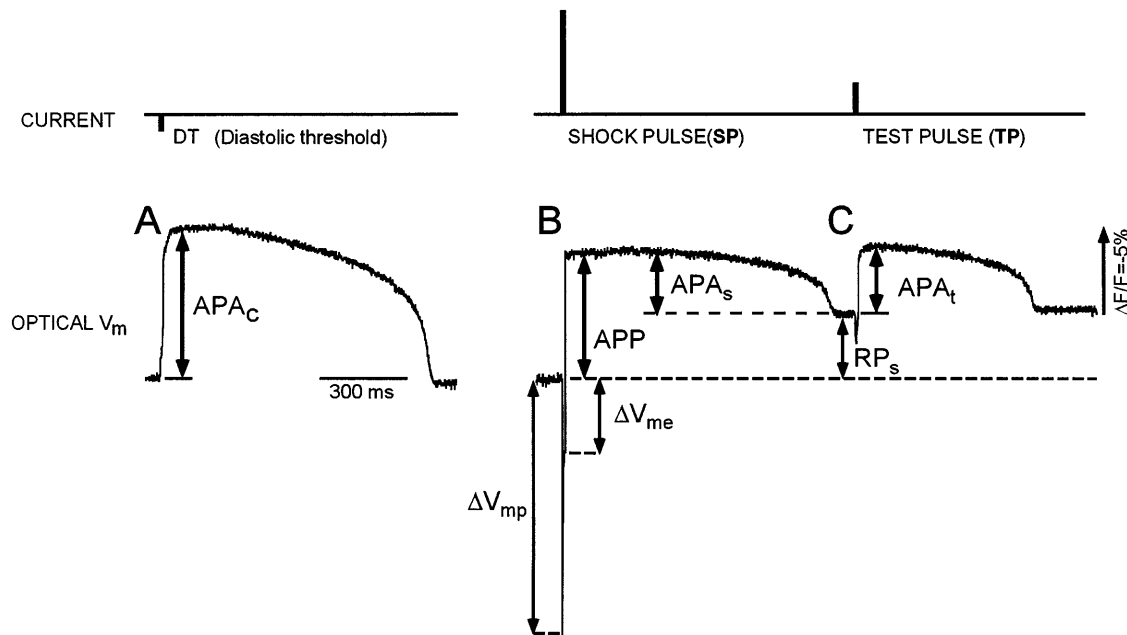


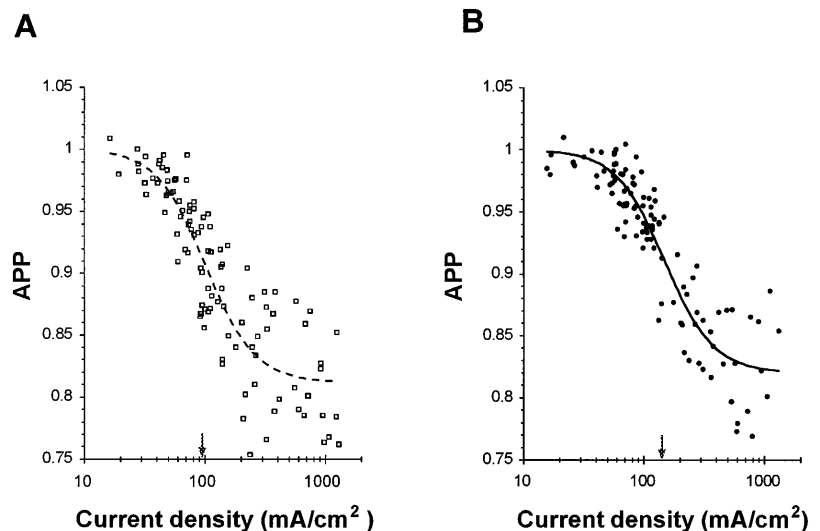
Fig. 3. Experimental protocol and terminology. Top trace, current applied through the stimulating electrode. Bottom trace, optical signal recorded directly under the stimulating electrode. Initially cathodal DT is determined and amplitude of induced action potential is measured ( $APA_c$ ). An SP (here an anodal pulse  $57 \times DT$ ) is then applied during diastole. Shock-induced action potential is characterized by the following parameters: APP amplitude,  $APA_s$ , and  $RP_s$ ; 1 s after the shock a test pulse (TP; usually an anodal pulse  $6 \times DT$ ) is applied. The subsequent action potential is characterized by its amplitude ( $APA_t$ ).  $V_m$ , transmembrane potential;  $\Delta V_{mp}$ , peak  $V_m$ ;  $\Delta V_{me}$ ,  $V_m$  at end of SP.  $\Delta F/F$ , percent change in fluorescent signal.

for values larger than  $\sim 200 \text{ mA/cm}^2$  or  $\sim 50 \times DT$ . These effects appeared even though the tissue under the recording optical fiber was largely immobilized with slight suction. It is known that high-intensity shock induces large and prolonged contraction (10). Therefore, only the recordings showing a characteristic action potential shape and a smooth repolarization to a steady baseline were analyzed.

Because the information on  $RP_s$  is redundant to the information given for APP and  $APA_s$  ( $RP_s = APP - APA_s$ ), it has not been plotted here. However, for both pulse polarities,  $RP_s$  increased sigmoidally with increasing shock intensity from a value of 0 to  $\sim 0.8$ .

$APA_s$  as a function of current density and pulse polarity.  $APA_s$  was measured 100 ms after the shock as a function of the pulse polarity and intensity. Figure 5, A and B, illustrates the relation between  $APA_s$  and SP current density for anodal and cathodal shocks, respectively. For both pulse polarities,  $APA_s$  decreased sigmoidally with increasing shock intensity from a value of 1 to  $\sim 0$ . As in the case for the analysis of APP, the data were fit by functions of the form of Eq. 1, which were then used to select subsets of data lying between 20 and 80% of the vertical range of the curve fits. The subsets of data were subjected to analysis of covariance, and the difference between  $ED_{50}$  values of the data (185 and

Fig. 4. Amplitude of APP induced by the shock as a function of shock current density for anodal and cathodal pulses. A: anodal shock data. Data were fit by the sigmoidal function of Eq. 1, which reaches an asymptote of  $(1 - a) = 0.81 \times APA_c$ . Half-maximum point of curve fit [50% effective dose ( $ED_{50}$ )] is indicated by arrow and was estimated by analysis of covariance (ANCOVA) to be  $94 \text{ mA/cm}^2$ . B: cathodal shock data. Data were fit by the sigmoidal function of Eq. 1, which reaches an asymptote of  $(1 - a) = 0.81 \times APA_c$ .  $ED_{50}$  is  $145 \text{ mA/cm}^2$ .



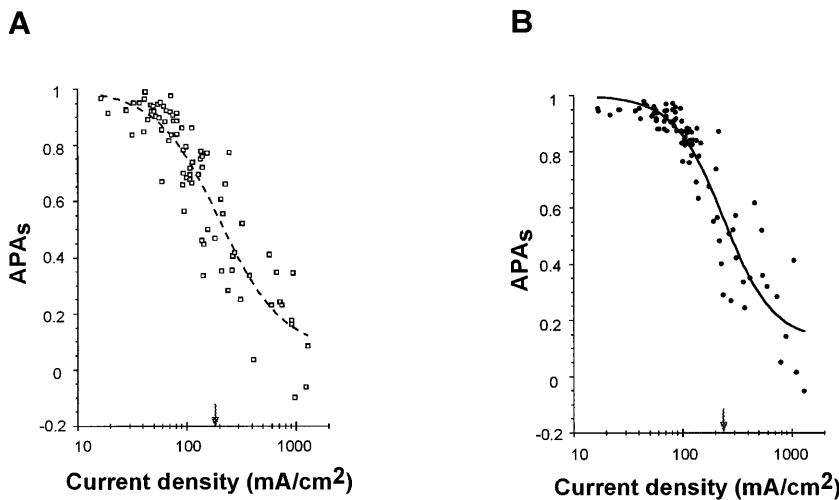


Fig. 5.  $APA_s$  as a function of the shock intensity for anodal and cathodal pulses. *A*: anodal shock data. Data were fit by sigmoidal function of Eq. 1, which reaches an asymptote of  $(1 - a) = 0.08 \times APA_c$ .  $ED_{50}$  is indicated by arrow and was estimated by ANCOVA to be 185 mA/cm<sup>2</sup>. *B*: cathodal shock data. Data were fit by sigmoidal function of Eq. 1, which reaches an asymptote of  $(1 - a) = 0.03 \times APA_c$ .  $ED_{50}$  is 238 mA/cm<sup>2</sup>.

238 mA/cm<sup>2</sup> for anodal and cathodal data, respectively) was found to be statistically significant ( $P = 0.02$ ). Therefore, on average the cathodal pulses required a higher intensity than the anodal pulses to induce a comparable change in  $APA_s$ .

To determine the electrical dosage needed to reduce  $APA_s$ , the threshold value was determined as the intercept of the linear fit to the  $APA_s$  dose-response curve, in the 20–80% range as previously described, with the horizontal line representing the mean value of  $APA_s$  at the lowest levels of shock intensities that were applied (0–10 mA/cm<sup>2</sup>). This analysis resulted in threshold values of 49 and 90 mA/cm<sup>2</sup> for the anodal and cathodal polarities, respectively.

*Recovery of the APA as a function of current density and pulse polarity.* The  $APA_t$  with TP intensity of  $6 \times DT$  delivered 1 s after SP was measured as a function of SP polarity and intensity. The results for  $APA_t$  were similar to those for  $APA_s$  presented in Fig. 5, although the half-maximal values for the data (256 and 329 mA/cm<sup>2</sup> for anodal and cathodal data, respectively) were significantly greater than those found for  $APA_s$  ( $P = 0.032$  for anodal and 0.028 for cathodal polarities). As was the case for  $APA_s$ , the data sets for  $APA_t$  for the two SP polarities were found to be significantly different from one another ( $P = 0.006$ ).

In experiments in which both  $APA_s$  and  $APA_t$  were measured for the same shock pulse, a recovery index (RI) defined (in %) as

$$RI = \frac{APA_t - APA_s}{APA_c - APA_s} \times 100 \quad (2)$$

was calculated to determine whether there was appreciable recovery of the APA during the 1-s interval after the SP. The data for RI are presented in Fig. 6 as a function of shock intensity. The data included both negative (indicating further degradation of APA) and positive (indicating recovery of APA) values of RI, and there did not appear to be a trend for RI as a function of shock intensity ( $r = 0.14$ ). These data also showed no significant dependence on polarity ( $z$  test,  $P > 0.15$  for anodal pulses and  $P > 0.27$  for cathodal pulses) but a marginally significant difference from zero (paired  $t$ -test,  $P = 0.063$ ). The mean of the pooled anodal and cathodal data ranged from 0 to 11% for a 90% confidence interval.

*$\Delta V_{mp}$  and  $\Delta V_{me}$  as a function of SP current density and polarity.* Both  $\Delta V_{mp}$  (Fig. 7A) and  $\Delta V_{me}$  (Fig. 7B) are plotted as a function of SP current density and polarity.  $\Delta V_{mp}$  was always negative for anodal pulses and positive for cathodal pulses. For anodal shocks,

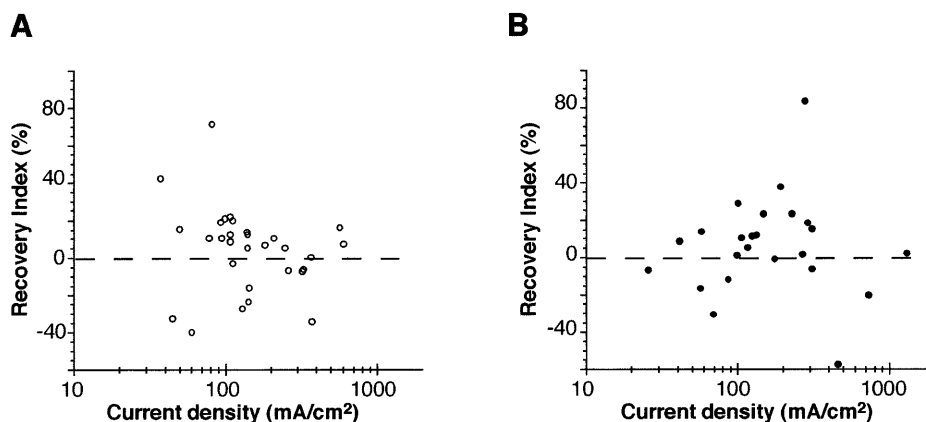
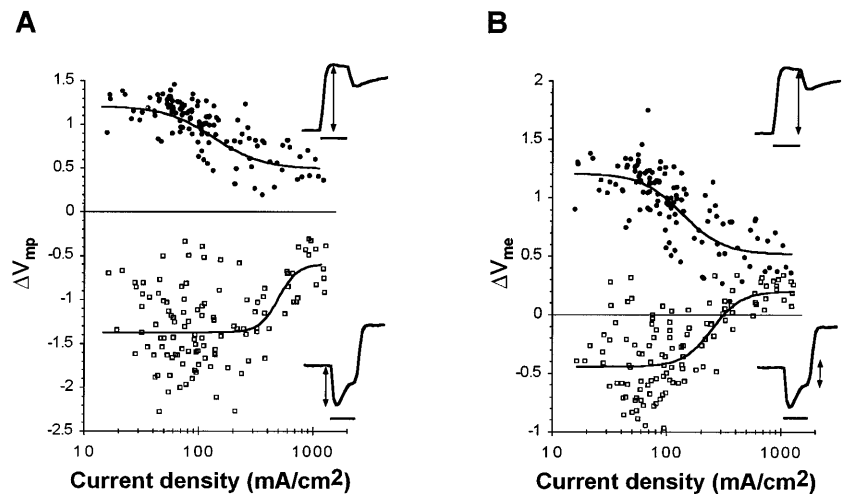


Fig. 6. Recovery index (RI) as a function of the shock intensity for anodal and cathodal pulses. RI is defined by Eq. 2 in text. *A*: anodal shock data. *B*: cathodal shock data.

Fig. 7. Changes in  $V_m$  ( $\Delta V_m$ ) induced by the shock as a function of shock intensity for anodal or cathodal pulses. Maximum changes in  $V_m$  ( $\Delta V_{mp}$ ) and  $V_m$  at end of the shock ( $\Delta V_{me}$ ) were measured. Horizontal line indicates time of the SP. *A*: relation of  $\Delta V_{mp}$  as a function of anodal and cathodal shock current density. For anodal shocks ( $\square$ )  $\Delta V_{mp}$  increases in magnitude to reach a maximum of about  $-2 \times \text{APA}_c$  and then decreases with increasing current density. For cathodal pulses ( $\bullet$ )  $\Delta V_{mp}$  remains constant and then decreases with increasing current density. *B*: relation of  $\Delta V_{me}$  as a function of anodal and cathodal shock current density.  $\Delta V_{me}$  converges at high current intensity toward a positive value for both anodal ( $\square$ ) and cathodal ( $\bullet$ ) SP.



$\Delta V_{mp}$  increased in amplitude with increasing SP intensities to a maximum value of about  $-2 \times \text{APA}_c$ . This maximum was reached at current densities of  $\sim 80$   $\text{mA}/\text{cm}^2$ . In the same intensity range,  $\Delta V_{mp}$  induced by cathodal pulses remained constant at a value of  $\sim 1.25 \times \text{APA}_c$ . For higher current densities,  $\Delta V_{mp}$  decreased in magnitude for both anodal and cathodal shocks, with a dependence of  $\Delta V_{me}$  on current densities similar to that for  $\Delta V_{mp}$ . In addition, for anodal SP intensities exceeding  $200\text{--}300$   $\text{mA}/\text{cm}^2$ ,  $\Delta V_{me}$  was positive, indicating membrane depolarization (Fig. 7*B*). At the very high current densities tested,  $\Delta V_{me}$  appeared to approach the same asymptotic value for both anodal and cathodal polarities.

## DISCUSSION

The main result of this study is that, under an extracellular electrode, electrical shocks applied in the whole ventricle during diastole alter various parameters of  $V_m$  as sigmoidal functions of the shock intensity. The half-maximal points of the functions depended on pulse polarity, with smaller values for the anodal pulses. The amplitude of the APP decreased toward a value of  $\sim 80\%$  of the  $\text{APA}_c$ , whereas the  $\text{RP}_s$  increased toward a value of  $\sim 80\%$   $\text{APA}_c$ . The  $\text{APA}_s$  decreased to zero, whereas the action potential measured 1 s after the shock ( $\text{APA}_t$ ) showed a marginal increase (i.e., recovery) compared with  $\text{APA}_s$ . Finally, the response of  $V_m$  during the shock pulse itself reached a maximum of about  $-2 \times \text{APA}_c$  during an anodal SP and to about  $1.25 \times \text{APA}_c$  during a cathodal SP, relative to the resting membrane potential.

The average current density of the cathodal diastolic threshold of excitation (Fig. 1) was determined to be  $3.9 \pm 1.3$   $\text{mA}/\text{cm}^2$  for a 10-ms monophasic rectangular pulse. The application of higher current densities for both anodal and cathodal shocks resulted in alterations in  $V_m$  that were sigmoidal functions of current density. The sigmoidal relation of the dose-response curves, taken together with the scatter of responses around the curve at a given shock level (Figs. 4–6), is highly suggestive of a probabilistic nature of membrane damage induced by electrical shock. This finding is reminis-

cent of the stochastic nature underlying electroporation (5) and is consistent with the hypothesis that electroporation is the underlying biophysical event. The threshold values for changes in APA were estimated to be  $\sim 49$   $\text{mA}/\text{cm}^2$  for anodal pulses and  $90$   $\text{mA}/\text{cm}^2$  for cathodal pulses. The  $\text{ED}_{50}$  values for reduction in APP were  $94$  and  $145$   $\text{mA}/\text{cm}^2$  with the anodal and cathodal polarities, respectively,  $185$  and  $238$   $\text{mA}/\text{cm}^2$  for reduction in  $\text{APA}_s$ , and  $256$  and  $329$   $\text{mA}/\text{cm}^2$  for reduction in  $\text{APA}_t$ . The progressive increase in these values for parameters measured with increasing delay after the delivery of the SP suggests that some form of recovery occurs immediately after the shock is applied. These values are comparable to those reported to produce mild arrhythmias in isolated rabbit hearts ( $0.5$   $\text{A}/\text{cm}^2$ ) but much smaller than that resulting in irreversible cell damage ( $1.8$   $\text{A}/\text{cm}^2$ ) (14). The differences may be due to the type and duration of waveform used (rectangular vs. damped sinusoid) or to the possibility that the electrophysiological changes that we observed are not irreversible. Indeed, we have previously reported recovery of APA over a period of tens of minutes after the application of a shock of  $118 \times \text{DT}$  (31), which, if taken as  $3.9$   $\text{mA}/\text{cm}^2$  from Fig. 2, is estimated to be  $\sim 460$   $\text{mA}/\text{cm}^2$ .

In most other studies of tissue injury that generally have involved cellular or muscle preparations, potential gradient rather than current density is the reported value. Previous experiments by Knisley et al. (13) on frog ventricular muscle showed significant effects on action potential amplitude and duration and on diastolic potential at field strengths of  $28\text{--}40$   $\text{V}/\text{cm}$  applied along the fiber axis. In this case, current density can be estimated by dividing the potential gradient by the longitudinal bulk resistivity, which is estimated to be  $\sim 204$   $\Omega \cdot \text{cm}$  from the data of Chapman and Fry (3), assuming longitudinal conductivities of  $588$  and  $75$   $\Omega \cdot \text{cm}$  in the intracellular and extracellular fiber spaces, respectively, and a ratio of 3:1 for intracellular to extracellular cross-sectional area. Hence, the data of Knisley et al. suggest that current densities on the order of  $140\text{--}200$   $\text{mA}/\text{cm}^2$  are sufficient to produce

electrophysiological dysfunction. These values are in the range of the  $ED_{50}$  values that we measured.

In addition, this study reveals asymmetric effects of the pulse polarity on the alterations of these parameters during diastole. Pulse polarity has been studied previously in the context of defibrillation threshold (2, 21) but not at high shock strengths. For identical current densities, our results show that anodal pulses have greater detrimental effects than do cathodal pulses. This finding of a greater effect of anodal pulses compared with cathodal pulses has been reported in previous studies involving electroporation and has been attributed either to the presence of the intrinsic negative resting potential that biases the membrane response in the negative direction (12, 24) or to electroosmosis (12). Another possibility is that during the pulse large depolarizations of the cell membrane will raise the membrane potential to an estimated value of +95 mV (Fig. 7), which is close enough to the reversal potential for Ca (estimated to be  $\sim 107$  mV from the Nernst equation, assuming an intracellular value of  $0.2 \mu\text{M}$ ) so that the electrochemical driving force for Ca entry would be close to zero. Conversely, large hyperpolarizations of the cell membrane would augment the electrochemical driving force for Ca entry and produce large inward Ca currents. Therefore, a large, asymmetric entry of Ca may occur that is aided by electroporation but biased by the positive Ca reversal potential and may contribute to the asymmetric effects of shock that we found in our study.

We found that with increasing current density the APP decreased toward an asymptotic value of  $\sim 0.81$   $APA_c$  (Fig. 4). This value corresponds to a membrane potential value of about +12 mV if we assume that the frog ventricular action potential has an amplitude of  $\sim 120$  mV and a resting potential of  $-85$  mV (13, 29). If electroporation is in fact the mechanism underlying the observed changes in plateau potential, the formation of nonselective pores in the cell membrane would be expected to depolarize the cell membrane toward a value of 0 mV once equilibration of ion concentrations has been reached (10, 25). However, the value of 12 mV observed in our study is not necessarily inconsistent with electroporation because the maximum current densities that were applied may not have been sufficiently high to electroporate all the cells in the optical recording volume or there may not have been sufficient time for equilibration of ions to have occurred.

A comparison of  $APA_t$  with  $APA_s$  gives some indication as to whether the membrane can recover during the 1-s time interval after SP. We found that RI showed a marginally significant difference from zero ( $P = 0.063$ ) and exhibited both positive and negative values irrespective of the shock intensity (Fig. 6). At a 90% confidence interval, the mean for RI was calculated to lie in the range of 0–11%. The limited recovery over this short interval is consistent with previous observations by us that recovery of APA takes place over tens of minutes after the application of a shock of  $118 \times DT$  (31). In addition, we have shown in a study of single frog ventricular cells (25) that after membrane break-

down was induced by a 5-ms rectangular shock, total recovery of membrane conductance occurred 3 min later in only 36% of the cells tested ( $n = 28$ ).

Our optical recording system allowed us to observe the response of the membrane potential during the shock pulse itself. With anodal pulses,  $\Delta V_{mp}$  reached a maximum value of  $-2 \times APA_c$  (Fig. 7A). This corresponds to a  $V_m$  of about  $-325$  mV (assuming that  $APA_c$  is  $\sim 120$  mV and that the resting potential lies at  $-85$  mV), which is sufficient to induce membrane electroporation (25). It should be pointed out that even larger membrane potentials may have occurred during the first millisecond of the shock pulse but were not observed because of the bandwidth limitation of our optical system. Therefore, our measurements of maximum values for  $\Delta V_{mp}$  may be underestimates of the true instantaneous voltage produced by SP.

With cathodal pulses,  $\Delta V_{mp}$  reaches a maximum value of  $1.25 \times APA_c$  from the resting potential, which corresponds to a membrane potential value of about +95 mV. Such a membrane potential value is insufficient to permeabilize the membrane (25), although as already discussed it is possible that larger potential changes exist but remain undetected. It is considerably smaller than that observed with anodal pulses ( $\sim 2 \times APA_c$ ), and such asymmetry between anodal and cathodal responses has been reported by us with 10-ms pulses applied during the plateau phase of the action potential (31). We speculate that the limitation in the voltage response in the positive potential range at levels below those expected for electroporation may result from several factors. First, it is possible that our potentiometric probe, di-4-ANEPPS, has a nonlinear response with transmembrane potential, particularly with large excursions out of the physiological range. This might be the result of alterations of the structural properties of the dye, saturation of the dye response, or electrophoresis of the dye into the membrane plasma. However, Hibino et al. (8), using a similar styryl dye (RH-292), have measured spatial variations in fluorescence (up to 50%) in sea urchin eggs in response to electrical fields of 67 V/cm that closely fitted the theoretical predictions of membrane response, provided that the response of the dye was linear with  $V_m$ . In addition, electrophoresis of the dye used in this study has been shown by Gross et al. (6) not to occur. Moreover, we see no change in fluorescence baseline with high shock even though the change in fluorescence induced by the pulse is reduced, suggesting that the dye response has not been altered by the high electric field.

A second possibility is that mechanisms other than electroporation may contribute to changes in membrane permeability. For example, in skeletal muscle fibers transmembrane potentials on the order of  $-600$  mV may alter Na and K conductance and ionic selectivity (4), although the voltage levels required to produce these changes were found to be larger than those for electroporation. It has been speculated that with large transmembrane potentials, protein channels may be denatured by Joule heating via the intense transmembrane currents or by electric modification of their

functional groups (26). Earlier work on red blood cells also has shown that suprphysiological transmembrane potentials can induce leakage currents across the cell membrane that are carried through the Na-K-adenosinetriphosphatase pathways (23).

A third factor that may contribute to the asymmetry in response is that we, and others, have previously shown that virtual electrodes of both polarities coexist near the stimulus electrode (11, 16) with a pattern that depends on the electrical anisotropy of the tissue. During cathodal stimulation, regions of secondary hyperpolarization will form adjacent to the central region directly under the electrode and will interact electrotonically as an electrical load. Because the electrical conductance of the membrane exhibits a well-known inward rectification, the high conductance of the hyperpolarized regions may act to limit the extent of depolarization of the central region. During anodal stimulation, a different mix of ion channels would be expected to be activated in the secondary depolarized regions now flanking the central region. Because channel conductances have been shown to influence the size and amplitude of the secondary polarized regions (19), which in turn alter the electrical loading conditions of the primary polarized region located directly under the electrode, differing magnitudes of responses might be expected for anodal vs. cathodal polarities.

A fourth possibility for the asymmetry in transmembrane potential response may be that there are unknown currents that are activated by the large polarization changes of the membrane that we have estimated earlier can vary between  $-325$  and  $+95$  mV. For example, it is possible that the known ionic channels alter their behavior outside the physiological range in which they have been characterized. Alternatively, there may be as yet unidentified ionic channels that await discovery, such as the recently described pacemaker-like current that activates at large hyperpolarized potentials in ventricular tissue (34).

Another unexpected finding was that the  $\Delta V_{me}$  induced by the shock converges toward a value of  $\sim 0.4$  APA<sub>c</sub> (Fig. 7B) for both pulse polarities at the highest current densities applied in this study. If the electropores generated during the shock are nonselective, i.e., aqueous filled pores with reversal potential of 0 mV, we would expect a convergence toward a value of  $\sim 0.7$  APA<sub>c</sub> (corresponding to  $\sim 0$  mV). The finding of a different value suggests that 1) electroporation is incomplete within the volume of tissue being recorded, 2) the electropores exhibit some specificity such that they have a negative reversal potential (estimated to be approximately  $-35$  mV), or 3) mechanisms other than electroporation (such as activation of an unknown channel with negative reversal potential) may be contributing to the observed response.

Application of high-intensity shock induces tissue depolarization and necrosis that can have pathophysiological consequences. Depolarization can create a region of conduction slowdown or block (33). This region could act as a focal point for reentrant-type arrhythmias and could also be responsible for the transient S-T

changes sometimes observed after cardioversion or defibrillation (1). Tissue depolarization would also be expected to alter pacing or defibrillation thresholds. In addition, the presence of depolarized regions could increase the excitability of adjacent tissue and consequently facilitate the formation of ectopic beats (7). Tissue necrosis could result in a change in tissue impedance, leading to apparent changes in cardioversion or defibrillation threshold that arise from the changes in current and voltage delivered from the device to the tissue.

In conclusion, this study reveals the detrimental effects of high-intensity shocks on the frog cardiac action potential directly under an extracellular stimulating electrode. These effects include reduction of APA and loss of RP, and these reductions increase sigmoidally with current density. In addition, there is a second-order dependence on pulse polarity, such that anodal pulses applied during diastole have a greater effect than cathodal pulses of the same intensity. These findings provide additional evidence to support the hypothesis that electroporation is a primary mechanism that underlies tissue damage induced by high-intensity shocks, although other mechanisms may also be involved.

We are grateful to Martin Beyerbach for assistance in the statistical analysis.

This work was supported by National Heart, Lung, and Blood Institute Grant HL-48266.

Address for reprint requests: L. Tung, Dept. of Biomedical Engineering, The Johns Hopkins Univ., 720 Rutland Ave., Baltimore, MD 21205.

Received 19 May 1997; accepted in final form 15 August 1997.

## REFERENCES

1. Avital, B., S. Port, R. Gal, J. McKinnie, P. Tchou, M. Jazayeri, P. Troup, and M. Akhtar. Automatic implantable cardioverter/defibrillator discharges and acute myocardial injury. *Circulation* 81: 1482-1487, 1990.
2. Bardy, G. H., T. D. Ivey, M. D. Allen, G. Johnson, and H. L. Greene. Evaluation of electrode polarity on defibrillation efficacy. *Am. J. Cardiol.* 63: 433-437, 1989.
3. Chapman, R. A., and C. H. Fry. An analysis of the cable properties of frog ventricular myocardium. *J. Physiol. (Lond.)* 283: 263-282, 1978.
4. Chen, W., and R. C. Lee. Altered ion channel conductance and ionic selectivity induced by large imposed membrane potential pulse. *Biophys. J.* 67: 603-617, 1994.
5. Freeman, S. A., M. A. Wang, and J. C. Weaver. Theory of electroporation on planar bilayer membranes: predictions of the aqueous area, change in capacitance, and pore-pore separation. *Biophys. J.* 67: 42-56, 1994.
6. Gross, D., L. M. Loew, and W. W. Webb. Optical imaging of cell membrane potential changes induced by applied electric fields. *Biophys. J.* 50: 339-348, 1986.
7. Hauer, R. N. W., J. M. T. de Bakker, A. A. M. de Wilde, S. Straks, J. T. Vermeulen, and M. J. Janse. Ventricular tachycardia after in vivo DC shock ablation in dogs. *Circulation* 84: 267-278, 1991.
8. Hibino, M., M. Itoh, and K. Kinoshita. Time course of cell electroporation as revealed by submicrosecond imaging of transmembrane potential. *Biophys. J.* 64: 1789-1800, 1993.
9. Jones, J. L. Waveforms for implantable cardioverter defibrillators (ICDs) and transchest defibrillation. In: *Defibrillation of the Heart: ICDs, AEDs, and Manual*, edited by W. A. Tacker. St. Louis, MO: Mosby, 1994, p. 46-81.

10. **Jones, J. L., R. E. Jones, and G. Balasky.** Microlesion formation in myocardial cells by high-intensity electric field stimulation. *Am. J. Physiol.* 253 (*Heart Circ. Physiol.* 22): H480–H486, 1987.
11. **Knisley, S. B.** Transmembrane voltage changes during unipolar stimulation of rabbit ventricle. *Circ. Res.* 77: 1229–1239, 1995.
12. **Knisley, S. B., and A. O. Grant.** Asymmetrical electrically induced injury of rabbit ventricular myocytes. *J. Mol. Cell. Cardiol.* 27: 1111–1122, 1995.
13. **Knisley, S. B., W. M. Smith, and R. E. Ideker.** Prolongation and shortening of action potentials by electrical shocks in frog ventricular muscle. *Am. J. Physiol.* 266 (*Heart Circ. Physiol.* 35): H2348–H2358, 1994.
14. **Koning, G., A. H. Veeffkind, and H. Schneider.** Cardiac damage caused by direct application of defibrillator shocks to isolated Langendorff-perfused rabbit heart. *Am. Heart J.* 100: 473–482, 1980.
15. **Neunlist, M., and L. Tung.** Optical recordings of ventricular excitability of frog heart by an extracellular stimulating point electrode. *Pacing Clin. Electrophysiol.* 17: 1641–1654, 1994.
16. **Neunlist, M., and L. Tung.** Spatial distribution of cardiac transmembrane potentials around an extracellular electrode. Dependence on fiber orientation. *Biophys. J.* 68: 2310–2322, 1995.
17. **Neunlist, M., S.-Z. Zou, and L. Tung.** Design and use of an “optrode” for optical recordings of cardiac action potentials. *Pflügers Arch.* 420: 611–617, 1992.
18. **O'Neill, R. J., and L. Tung.** Cell-attached patch clamp study of the electroporation of amphibian cardiac cells. *Biophys. J.* 59: 1028–1039, 1991.
19. **Roth, B. J., and J. P. J. Wikswo.** Electrical stimulation of cardiac tissue: a bidomain model with active membrane properties. *IEEE Trans. Biomed. Eng.* 41: 232–240, 1994.
20. **Salama, G.** Optical measurement of transmembrane potential in heart. In: *Spectroscopic Membrane Probes*, edited by L. Loew. Boca Raton, FL: CRC, 1988, vol. III, p. 137–199.
21. **Schuder, J. C., H. Stoeckle, W. C. McDaniel, and M. Dbeis.** Is the effectiveness of cardiac ventricular defibrillation dependent upon polarity? *Med. Instr.* 21: 262–265, 1987.
22. **Tang, A. S. L., P. D. Wolf, Y. Afework, W. M. Smith, and R. E. Ideker.** Three-dimensional potential gradient fields generated by intracardiac catheter and cutaneous patch electrode. *Circulation* 85: 1857–1864, 1992.
23. **Teissie, J., and T. Y. Tsong.** Evidence of voltage-induced channel opening in Na/K ATPase of human erythrocyte membrane. *J. Membr. Biol.* 55: 133–140, 1980.
24. **Tekle, E., R. D. Astumian, and P. B. Chock.** Electroporation of cell membranes: effect of the resting membrane potential. *Biochem. Biophys. Res. Commun.* 172: 282–287, 1990.
25. **Tovar, O., and L. Tung.** Electroporation and recovery of the cardiac cell membrane with rectangular voltage pulses. *Am. J. Physiol.* 263 (*Heart Circ. Physiol.* 32): H1128–H1136, 1992.
26. **Tsong, T. Y.** Electroporation of cell membranes. *Biophys. J.* 60: 297–306, 1991.
27. **Tung, L.** Deleterious effects of electrical fields on cardiac muscle. *Proc. IEEE* 84: 366–378, 1996.
28. **Tung, L.** Electrical injury to heart muscle cells. In: *Electrical Trauma: The Pathophysiology, Manifestations, and Clinical Management*, edited by R. C. Lee, E. G. Cravalho, and J. F. Burke. Cambridge, UK: University of Cambridge Press, 1992, p. 361–400.
29. **Tung, L., and M. Morad.** A comparative electrophysiological study of enzymatically isolated single cells and strips of frog ventricle. *Pflügers Arch.* 405: 274–284, 1985.
30. **Tung, L., and M. Neunlist.** Asymmetrical injury effects of high intensity anodal and cathodal shock on cardiac transmembrane potentials (Abstract). *Am. Heart J.* 128: 634, 1994.
31. **Tung, L., O. Tovar, M. Neunlist, S. K. Jain, and R. J. O'Neill.** Effects of strong electrical shock on cardiac muscle tissue. *Ann. NY Acad. Sci.* 720: 160–175, 1994.
32. **Wharton, J. M., P. D. Wolf, W. M. Smith, P.-S. Chen, D. W. Frazier, S. Yabe, N. Danieleley, and R. E. Ideker.** Cardiac potential and potential gradient fields generated by single, combined, and sequential shocks during ventricular defibrillation. *Circulation* 85: 1510–1523, 1992.
33. **Yabe, S., W. M. Smith, J. P. Daubert, P. D. Wolf, D. L. Rollins, and R. E. Ideker.** Conduction disturbances caused by high current density electric fields. *Circ. Res.* 66: 1190–1203, 1990.
34. **Yu, H., F. Chang, and I. S. Cohen.** Pacemaker current  $i(f)$  in adult cardiac ventricular myocytes. *J. Physiol. (Lond.)* 485: 469–483, 1995.